

First Homologous Series of Iron Pnictide Oxide Superconductors

(Fe₂As₂)(Ca_{n+1}(Sc,Ti)_nO_y) [*n* = 3,4,5] with Extremely Thick Blocking Layers

Hiraku Ogino^{1,3,a}, Shinya Sato^{1,3}, Kohji Kishio^{1,3}, Jun-ichi Shimoyama^{1,3}, Tetsuya Tohei², and
Yuichi Ikuhara²

¹Department of Applied Chemistry, The University of Tokyo, 7-3-1 Hongo, Bunkyo-ku,
Tokyo 113-8656, Japan

²Institute of Engineering Innovation, The University of Tokyo, 2-11-16 Yayoi, Bunkyo-ku,
Tokyo 113-8656, Japan

³JST-TRIP, Sanban-cho, Chiyoda-ku, Tokyo 102-0075, Japan

a) Electronic mail: tuogino@mail.ecc.u-tokyo.ac.jp

We have discovered first homologous series of iron pnictide oxide superconductors $(\text{Fe}_2\text{As}_2)(\text{Ca}_{n+1}(\text{Sc,Ti})_n\text{O}_y)$ [$n = 3,4,5$]. These compounds have extremely thick blocking layers up to quintuple perovskite oxide layers sandwiched by the Fe_2As_2 layers. These samples exhibited bulk superconductivity with relatively high T_c up to 42 K. The relationship between T_c and the iron-plane interlayer distance suggested that superconductivity due to the mono Fe_2As_2 layer is substantially 40 K-class.

In a recently discovered layered iron pnictide family¹, the superconducting transition temperature T_c increased under ambient pressure in the order of FeSe ($T_c = 8\text{-}13$ K, $d = 5.49$ Å)², $(\text{Ba,K})\text{Fe}_2\text{As}_2$ (38 K, 6.65 Å)³ and $\text{SmFeAs}(\text{O,F})$ (55 K, 8.44 Å)⁴, where d represents the distance between the iron-planes. This suggested that emphasis of two-dimensionality by an increase of the interlayer distance of superconducting planes would be a promising method to develop new high- T_c superconductors. On the other hand, a new family of layered iron pnictides with perovskite-type oxide blocking layers has recently been discovered⁵⁻¹². The thickness of the perovskite-type layer can be controlled according to the composition and the synthesis conditions; therefore, an attempt to develop new layered iron pnictides with thicker oxide layers may result in a new series of homologous superconductors. Novel compounds with double or triple perovskite layers were discovered in our recent study, such as $(\text{Fe}_2\text{As}_2)(\text{Ba}_3\text{Sc}_2\text{O}_5)$ and $(\text{Fe}_2\text{As}_2)(\text{Sr}_4(\text{Sc,Ti})_3\text{O}_8)$ ¹². These new compounds indicated that a perovskite layer, which can maintain electroneutrality with the $(\text{Fe}_2\text{As}_2)^{-2}$ layer and have an appropriate lattice size $a \sim 4$ Å, can form layered iron pnictide oxides. According to these

empirical observations, three new compounds with different crystal structures, $(\text{Fe}_2\text{As}_2)(\text{Ca}_{n+1}(\text{Sc,Ti})_n\text{O}_y)$ [$n = 3,4,5$ and $y \sim 3n-1$] were discovered.

Samples were synthesized by solid-state reaction from starting materials of FeAs (3N), Ca (2N), CaO (2N), Ti (3N), TiO_2 (3N) and Sc_2O_3 (3N). The starting reagents were moisture sensitive, so that manipulation was carried out in a glove box filled with argon gas. Powder mixtures were pelletized, sealed in evacuated quartz ampoules and heated at 1000-1200 °C for 60-100 h followed by slow cooling to room temperature.

Phase identification was carried out using powder XRD (Rigaku Ultima-IV) and intensity data were collected in the 2θ range of 3-80° at a step of 0.02° using $\text{Cu-K}\alpha$ radiation. High resolution TEM images were taken using JEM-2010F and JEM-4010 (JEOL). Magnetic susceptibility was measured using a superconducting quantum interference device (SQUID) magnetometer (Quantum Design MPMS-XL5s). Electrical resistivity was evaluated by the AC four-point-probe method (Quantum Design PPMS).

$(\text{Fe}_2\text{As}_2)(\text{Ca}_4(\text{Sc}_{0.67}\text{Ti}_{0.33})_3\text{O}_y)$, $(\text{Fe}_2\text{As}_2)(\text{Ca}_5(\text{Sc}_{0.5}\text{Ti}_{0.5})_4\text{O}_y)$ and $(\text{Fe}_2\text{As}_2)(\text{Ca}_6(\text{Sc}_{0.4}\text{Ti}_{0.6})_5\text{O}_y)$ samples were successfully obtained by sintering for 72 h at 1050, 1100 and 1200 °C, respectively. Each compound formed as a main phase with small amounts of impurities, such as CaFe_2As_2 , FeAs and CaSc_2O_4 , as shown in XRD patterns of Fig. 1. The half unit cell crystal structures of these new compounds are shown in Fig. 2. Their unit cells are tetragonal with a space group of $I4/mmm$. $(\text{Fe}_2\text{As}_2)(\text{Ca}_4(\text{Sc}_{0.67}\text{Ti}_{0.33})_3\text{O}_y)$ has the same

crystal structure as $(\text{Fe}_2\text{As}_2)(\text{Sr}_4(\text{Sc},\text{Ti})_3\text{O}_8)^{12}$. In contrast, the crystal structures of $(\text{Fe}_2\text{As}_2)(\text{Ca}_5(\text{Sc}_{0.5}\text{Ti}_{0.5})_4\text{O}_y)$ and $(\text{Fe}_2\text{As}_2)(\text{Ca}_6(\text{Sc}_{0.4}\text{Ti}_{0.6})_5\text{O}_y)$ have new crystal structure with four and five perovskite layers, respectively, between the Fe_2As_2 layers. It should be noted that compounds with larger number of perovskite layers form at higher temperatures. The lattice constants determined from the XRD data were $a = 3.922 \text{ \AA}$ and $c/2 = 16.78 \text{ \AA}$ for $(\text{Fe}_2\text{As}_2)(\text{Ca}_4(\text{Sc}_{0.67}\text{Ti}_{0.33})_3\text{O}_y)$, $a = 3.902 \text{ \AA}$ and $c/2 = 20.63 \text{ \AA}$ for $(\text{Fe}_2\text{As}_2)(\text{Ca}_5(\text{Sc}_{0.5}\text{Ti}_{0.5})_4\text{O}_y)$, and $a = 3.884 \text{ \AA}$ and $c/2 = 24.58 \text{ \AA}$ for $(\text{Fe}_2\text{As}_2)(\text{Ca}_6(\text{Sc}_{0.4}\text{Ti}_{0.6})_5\text{O}_y)$. The half c -axis length increased by $\sim 3.9 \text{ \AA}$ due to a one perovskite layer increase in the half unit cell, which is reasonable, because the lattice constant of cubic $\text{Ca}(\text{Sc},\text{Ti})\text{O}_3$ is $\sim 3.9 \text{ \AA}$. It should be noted that $(\text{Fe}_2\text{As}_2)(\text{Ca}_6(\text{Sc}_{0.4}\text{Ti}_{0.6})_5\text{O}_y)$ has the longest interlayer distance of the iron planes in the layered iron pnictide oxides at $\sim 24.6 \text{ \AA}$. On the other hand, small shortenings in the a -axis length can be explained by the difference in the ratio of scandium and titanium, because the ionic radius of Sc^{3+} is slightly larger than that of Ti^{4+} .

If all the oxygen sites are fully occupied, then the oxygen content y in $(\text{Fe}_2\text{As}_2)(\text{Ca}_4\text{M}_3\text{O}_y)$, $(\text{Fe}_2\text{As}_2)(\text{Ca}_5\text{M}_4\text{O}_y)$ and $(\text{Fe}_2\text{As}_2)(\text{Ca}_6\text{M}_5\text{O}_y)$ is 8, 11 and 14, respectively. However, the samples synthesized from nominal oxygen contents of $y = 8, 11$ and 14 exhibited very low phase purity with large amounts of CaTiO_3 and other phases present. The samples shown in Fig. 1 were synthesized from the oxygen deficient nominal compositions $(\text{Fe}_2\text{As}_2)(\text{Ca}_4(\text{Sc}_{0.67}\text{Ti}_{0.33})_3\text{O}_{7.5})$, $(\text{Fe}_2\text{As}_2)(\text{Ca}_5(\text{Sc}_{0.5}\text{Ti}_{0.5})_4\text{O}_{10})$ and $(\text{Fe}_2\text{As}_2)(\text{Ca}_6(\text{Sc}_{0.4}\text{Ti}_{0.6})_5\text{O}_{13})$. Starting from oxygen deficient compositions with titanium in the lower valence state during the early stage of the reaction might be crucial to form the layered pnictide oxides, because

tetravalent titanium tends to form CaTiO_3 , which is a stable compound. Although the oxygen contents in the resulting samples are difficult to determine, they are considered to be close to 8, 11 or 14, respectively. The partial brown coloring of the quartz ampoule after the reaction suggested that a certain amount of oxygen is supplied to the samples by the partial decomposition of SiO_2 . The mean valences of the cations at the M -site were calculated to be +3.33, +3.50 and +3.60 in $(\text{Fe}_2\text{As}_2)(\text{Ca}_4\text{M}_3\text{O}_8)$, $(\text{Fe}_2\text{As}_2)(\text{Ca}_5\text{M}_4\text{O}_{11})$ and $(\text{Fe}_2\text{As}_2)(\text{Ca}_6\text{M}_5\text{O}_{14})$, respectively, by taking electroneutrality into account. Since the valences of scandium and titanium ions in these samples are considered to be +3 and +4, respectively, the atomic ratio of scandium and titanium is almost uniquely determined in each phase; 2:1 for $(\text{Fe}_2\text{As}_2)(\text{Ca}_4\text{M}_3\text{O}_8)$, 1:1 for $(\text{Fe}_2\text{As}_2)(\text{Ca}_5\text{M}_4\text{O}_{11})$ and 2:3 for $(\text{Fe}_2\text{As}_2)(\text{Ca}_6\text{M}_5\text{O}_{14})$. Samples starting from different ratios of scandium and titanium always contained larger amounts of impurity phases and the variation of lattice constants by changing the scandium/titanium ratio was confirmed to be small. If the scandium/titanium ratio is expressed as $(1-x):x$, then the relationship between n and x is calculated as $x = 1-2/n$. Therefore, the general formula of the present system is expressed as $(\text{Fe}_2\text{As}_2)(\text{Ca}_{n+1}(\text{Sc}_{2/n}\text{Ti}_{1-2/n})_n\text{O}_{3n-1})$. Further increase in the thickness of the blocking layer, *i.e.*, an increase in n , would be possible by tuning the scandium/titanium ratio according to the general formula and synthesis at higher temperatures.

Figure 3 shows high resolution transmission electron microscopy (TEM) images and electron diffraction (ED) patterns taken from the [100] direction of $(\text{Fe}_2\text{As}_2)(\text{Ca}_4(\text{Sc}_{0.67}\text{Ti}_{0.33})_3\text{O}_y)$ and $(\text{Fe}_2\text{As}_2)(\text{Ca}_5(\text{Sc}_{0.5}\text{Ti}_{0.5})_4\text{O}_y)$ crystals. Both TEM images and

ED patterns indicate a tetragonal cell with c/a of ~ 4.1 for $(\text{Fe}_2\text{As}_2)(\text{Ca}_4(\text{Sc}_{0.67}\text{Ti}_{0.33})_3\text{O}_y)$ and ~ 5.2 for $(\text{Fe}_2\text{As}_2)(\text{Ca}_5(\text{Sc}_{0.5}\text{Ti}_{0.5})_4\text{O}_y)$. These values correspond well with the values estimated from the XRD analysis; $c/a \sim 4.3$ and 5.3 . No stacking faults or superstructures were found along the c -axis direction in either crystals. On the other hand, the ED pattern suggested the existence of a superstructure along the a -axis in both crystals with a period of $2a$. An ordered configuration of scandium and titanium in the crystal is not the origin of the superstructure, because the superstructure was found in $(\text{Fe}_2\text{As}_2)(\text{Ca}_4(\text{Sc}_{0.67}\text{Ti}_{0.33})_3\text{O}_y)$ where the ratio of scandium to titanium is 2:1. In addition, such satellite spots were not observed in the ED pattern of $(\text{Fe}_2\text{As}_2)(\text{Sr}_4(\text{Mg}_{0.5}\text{Ti}_{0.5})_2\text{O}_6)^{12}$. Therefore, the observed superstructure is probably due to local periodic lattice deformations.

The temperature dependence of the zero-field-cooled (ZFC) and field-cooled (FC) magnetization curves of $(\text{Fe}_2\text{As}_2)(\text{Ca}_4(\text{Sc}_{0.67}\text{Ti}_{0.33})_3\text{O}_y)$, $(\text{Fe}_2\text{As}_2)(\text{Ca}_5(\text{Sc}_{0.5}\text{Ti}_{0.5})_4\text{O}_y)$ and $(\text{Fe}_2\text{As}_2)(\text{Ca}_6(\text{Sc}_{0.4}\text{Ti}_{0.6})_5\text{O}_y)$ measured under 1 Oe are shown in Fig. 4(a). All of the compounds exhibited large diamagnetism, which suggests superconductivity. The $T_{c(\text{onset})}$'s were ~ 36 K for $(\text{Fe}_2\text{As}_2)(\text{Ca}_5(\text{Sc}_{0.5}\text{Ti}_{0.5})_4\text{O}_y)$ and $(\text{Fe}_2\text{As}_2)(\text{Ca}_6(\text{Sc}_{0.4}\text{Ti}_{0.6})_5\text{O}_y)$ and 31 K for $(\text{Fe}_2\text{As}_2)(\text{Ca}_4(\text{Sc}_{0.67}\text{Ti}_{0.33})_3\text{O}_y)$. The superconducting volume fraction estimated from the ZFC magnetization at 2 K was much larger than the perfect diamagnetism due to the demagnetization effect and the porous microstructure with closed pores. The reversible magnetization observed down to several K below the $T_{c(\text{onset})}$ suggested poor grain coupling and weak intragrain pinning at high temperatures.

Figure 4(b) shows the temperature dependence of resistivity for

(Fe₂As₂)(Ca₄(Sc_{0.67}Ti_{0.33})₃O_y), (Fe₂As₂)(Ca₅(Sc_{0.5}Ti_{0.5})₄O_y) and (Fe₂As₂)(Ca₆(Sc_{0.4}Ti_{0.6})₅O_y), with resistivity curves from 25 to 50 K in the inset. All three samples exhibited metallic behavior in the normal state with respective $T_{c(\text{onset})}$'s of approximately 33, 41 and 42 K. The broad transitions observed for all samples are partly explained by poor grain coupling; however, apparently higher $T_{c(\text{onset})}$'s than those observed in the magnetization measurements may indicate the effect of superconductivity fluctuation near T_c .

In the series of newly discovered compounds (Fe₂As₂)(Ca_{*n*+1}(Sc,Ti)_{*n*}O_{*y*}) [*n* = 3,4,5 and *y* ~3*n*-1], superconducting Fe₂As₂ layers are largely separated from each other by the thick perovskite oxide layers. To our knowledge, the interlayer distance between the iron planes, *d* ~24.6 Å, of (Fe₂As₂)(Ca₆(Sc_{0.4}Ti_{0.6})₅O_{*y*}) is the longest among all superconductors, except for artificially deposited multi-layer films. It should be noted that *d* of layered iron-based superconductors can be changed from ~5 Å for FeSe² to 24.6 Å. The variation of *d* is much larger than other layered superconductors, such as cuprate superconductors, which indicates the high chemical stability and structural flexibility of the Fe₂As₂ layer. The $T_{c(\text{onset})}$'s of the iron pnictides and chalcogenides^{1,3,4,6,9,10,13-20} are plotted as a function of the interlayer distance *d* in Fig. 5. In this plot, superconductors having a doped iron plane were excluded, because such compounds usually exhibit lower T_c due to structural and/or electronic disorder in the superconducting layer. No systematic dependence of T_c on *d* was found, but T_c seems almost constant at ~40 K when *d* > 15 Å. In other words, the dimensionality of the crystal structure is not a major factor in determining T_c of layered iron-based superconductors. The coherence length in the *c*-axis direction, ξ_c , of the 1111 compound is reported to be 4.5 Å²¹.

Although ξ_c of the $(\text{Fe}_2\text{As}_2)(\text{Ca}_{n+1}(\text{Sc,Ti})_n\text{O}_y)$ series has not been evaluated, it is believed to be shorter than that of the 1111 compound, due to the thick blocking layers. Therefore, superconductivity in $(\text{Fe}_2\text{As}_2)(\text{Ca}_{n+1}(\text{Sc,Ti})_n\text{O}_y)$ compounds is considered to originate from completely separated Fe_2As_2 layers, which inherently exhibit 40 K-class T_c . The particularly high T_c of the 1111 compounds may be due to moderate interaction between the Fe_2As_2 layers.

New iron pnictide oxide superconductors with extremely thick blocking layers $(\text{Fe}_2\text{As}_2)(\text{Ca}_{n+1}(\text{Sc,Ti})_n\text{O}_y)$ [$n = 3,4,5$ and $y \sim 3n-1$] were discovered in the present study. These samples exhibited bulk superconductivity with relatively high T_c up to 42 K. The relationship between T_c and the iron-plane interlayer distance suggested that superconductivity due to the mono Fe_2As_2 layer is substantially 40 K-class. It is thought that there is still considerable room for the development of new layered iron pnictide compounds, due to the structural and chemical flexibility of the blocking layer. However, the present results suggest that optimization of the local structure of Fe_2As_2 layers and the dimensionality of the crystal structure may not lead to further enhancement of T_c . Other challenging approaches, such as the introduction of double superconducting layers, will be required for a new breakthrough in T_c .

This work was supported in part by the Ministry of Education, Culture, Sports, Science, and Technology (MEXT), Japan, through a Grant-in-Aid for Young Scientists (B) (No. 21750187).

1. Y. Kamihara, T. Watanabe, M. Hirano, and H. Hosono, *J. Am. Chem. Soc.*, **130**, 3296 (2008).
2. F. C. Hsu, J. Y. Luo, K. W. The, T. K. Chen, T. W. Huang, P. M. Wu, Y. C. Lee, Y. L. Huang, Y. Y. Chu, D. C. Yan, and M. K. Wu, *Proc. Nat. Acad. Sci. U.S.A.* **105**, 14262 (2008).
3. M. Rotter, M. Tegel, and D. Johrendt, *Phys. Rev. Lett.* **101**, 107006 (2008).
4. Z. A. Ren, W. Lu, J. Yang, W. Yi, X. L. Shen, C. Zheng, G. C. Che, X. L. Dong, L. L. Sun, F. Zhou, and Z. X. Zhao, *Chin. Phys. Lett.* **25**, 2215 (2008).
5. X. Zhu, F. Han, G. Mu, B. Zeng, P. Cheng, B. Shen, and H. H. Wen, *Phys. Rev. B* **79**, 024516 (2009).
6. H. Ogino, Y. Matsumura, Y. Katsura, K. Ushiyama, S. Horii, K. Kishio and J. Shimoyama *Supercond. Sci. Technol.* **22**, 075008 (2009).
7. H. Ogino, Y. Katsura, S. Horii, K. Kishio and J. Shimoyama *Supercond. Sci. Technol.* **22**, 085001 (2009).
8. G. F. Chen, T. L. Xia, H. X. Yang, J. Q. Li, P. Zheng, J. L. Luo, and N. L. Wang *Supercond. Sci. Technol.* **22**, 072001 (2009).
9. X. Zhu, F. Han, G. Mu, P. Cheng, B. Shen, B. Zeng, and H. H. Wen *Phys. Rev. B* **79**, 220512(R) (2009).
10. S. Sato, H. Ogino, N. Kawaguchi, Y. Katsura, K. Kishio, and J. Shimoyama, *Supercond. Sci. Technol.*, **23**, 045001 (2010).
11. H. Kotegawa, T. Kawazoe, H. Tou, K. Murata, H. Ogino, K. Kishio, and J. Shimoyama *J. Phys. Soc. Jpn.* **78**, 123707 (2009).
12. N. Kawaguchi, H. Ogino, Y. Shimizu, K. Kishio, and J. Shimoyama, *J. APEX* **3**, 063102

(2010)

13. Margadonna, S. *et al. Phys. Rev. B* **80**, 064506 (2009).
14. M. Tegel, C. Lohnert, and D. Johrendt, *Solid State Comm.* **150**, 383 (2010).
15. M. J. Pitcher, D. R. Parker, P. Adamson, S. J. C. Herkelrath, A. T. Boothroyd, and S. J. Clarke *Chem. Comm.* **45**, 5918 (2008).
16. D. R. Parker, M. J. Pitcher, and S. J. Clarke *Chem. Comm.* **16**, 2189 (2009).
17. S. Jiang, H. Xing, G. Xuan, C. Wang, Z. Ren, C. Feng, J. Dai, Z. Xu, and G. Cao, *J. Phys.: Condens. Matter* **21**, 382203 (2009).
18. C.H. Lee, H. Eisaki, H. Kito, M.T. Fernandez-Diaz, T. Ito, K. Kihou, H. Matsushita, M. Braden, and K. Yamada, *J. Phys. Soc. Jpn.* **77**, 083704 (2008).
19. R. Kumai, N. Takashita, T. Ito, H. Kito, A. Iyo, and H. Eisaki *J. Phys. Soc. Jpn.* **78**, 013705 (2009).
20. K. Miyazawa, K. Kihou, P. M. Shirage, C. H. Lee, H. Kito, H. Eisaki, and A. Iyo, *J. Phys. Soc. Jpn.* **78**, 034712 (2009).
21. M. Putti, I. Pallecchi, E. Bellingeri, M. R. Cimberle, M. Tropeano, C Ferdeghini, A. Palenzona, C. Tarantini, A. Yamamoto, J. Jiang, J. Jaroszynski, F. Kametani, D. Abraimov, A. Polyanskii, J. D. Weiss, E. E. Hellstrom, A. Gurevich, D. C. Larbalestier, R. Jin, B. C. Sales, A. S. Sefat, M. A. McGuire, D. Mandrus, P. Cheng, Y. Jia, H. H. Wen, S. Lee, and C. B. Eom, *Supercond. Sci. Technol.* **23**, 034003 (2010).

Figure captions

Figure 1. Powder XRD patterns of (a) $(\text{Fe}_2\text{As}_2)(\text{Ca}_4(\text{Sc}_{0.67}\text{Ti}_{0.33})_3\text{O}_y)$, (b) $(\text{Fe}_2\text{As}_2)(\text{Ca}_5(\text{Sc}_{0.5}\text{Ti}_{0.5})_4\text{O}_y)$, and (c) $(\text{Fe}_2\text{As}_2)(\text{Ca}_6(\text{Sc}_{0.4}\text{Ti}_{0.6})_5\text{O}_y)$.

Figure 2. Crystal structures of (a) $(\text{Fe}_2\text{As}_2)(\text{Ca}_4(\text{Sc},\text{Ti})_3\text{O}_8)$, (b) $(\text{Fe}_2\text{As}_2)(\text{Ca}_5(\text{Sc},\text{Ti})_4\text{O}_{11})$, and (c) $(\text{Fe}_2\text{As}_2)(\text{Ca}_6(\text{Sc},\text{Ti})_5\text{O}_{14})$.

Figure 3. High resolution TEM images and corresponding ED patterns of (a) $(\text{Fe}_2\text{As}_2)(\text{Ca}_4(\text{Sc}_{0.67}\text{Ti}_{0.33})_3\text{O}_y)$ and (b) $(\text{Fe}_2\text{As}_2)(\text{Ca}_5(\text{Sc}_{0.5}\text{Ti}_{0.5})_4\text{O}_y)$ crystals viewed from the [100] direction.

Figure 4. Superconducting properties. (a) Temperature dependence of ZFC and FC magnetization curves for $(\text{Fe}_2\text{As}_2)(\text{Ca}_4(\text{Sc}_{0.67}\text{Ti}_{0.33})_3\text{O}_y)$, $(\text{Fe}_2\text{As}_2)(\text{Ca}_5(\text{Sc}_{0.5}\text{Ti}_{0.5})_4\text{O}_y)$ and $(\text{Fe}_2\text{As}_2)(\text{Ca}_6(\text{Sc}_{0.4}\text{Ti}_{0.6})_5\text{O}_y)$ bulk samples measured under 1 Oe. (b) Temperature dependence of resistivity for bulk $(\text{Fe}_2\text{As}_2)(\text{Ca}_4(\text{Sc}_{0.67}\text{Ti}_{0.33})_3\text{O}_y)$, $(\text{Fe}_2\text{As}_2)(\text{Ca}_5(\text{Sc}_{0.5}\text{Ti}_{0.5})_4\text{O}_y)$ and $(\text{Fe}_2\text{As}_2)(\text{Ca}_6(\text{Sc}_{0.4}\text{Ti}_{0.6})_5\text{O}_y)$. Magnified resistivity curves are shown in the inset.

Figure 5. Relationship between T_c and the iron-plane interlayer distance for various layered iron pnictides.

Fig. 1

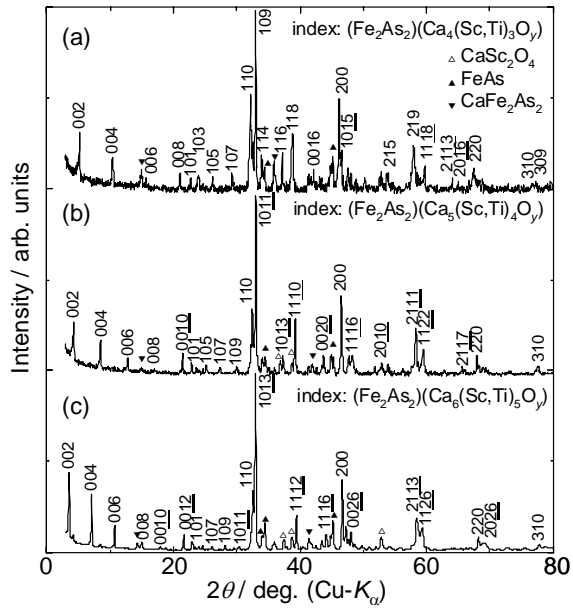


Fig. 2

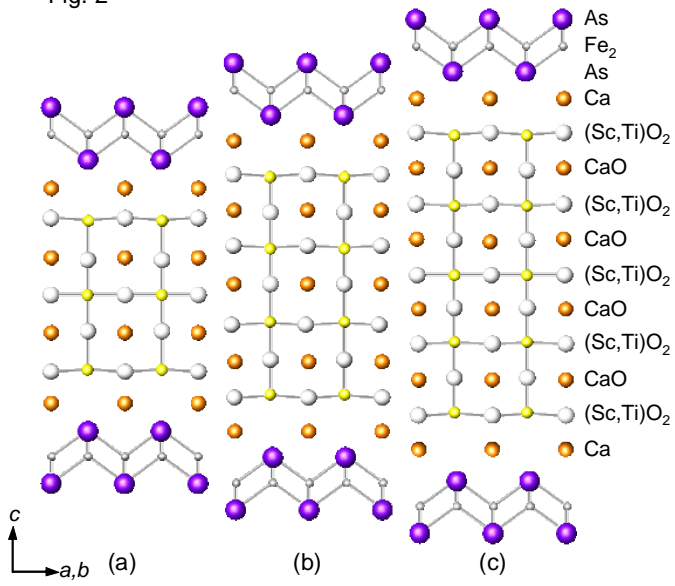


Fig. 3

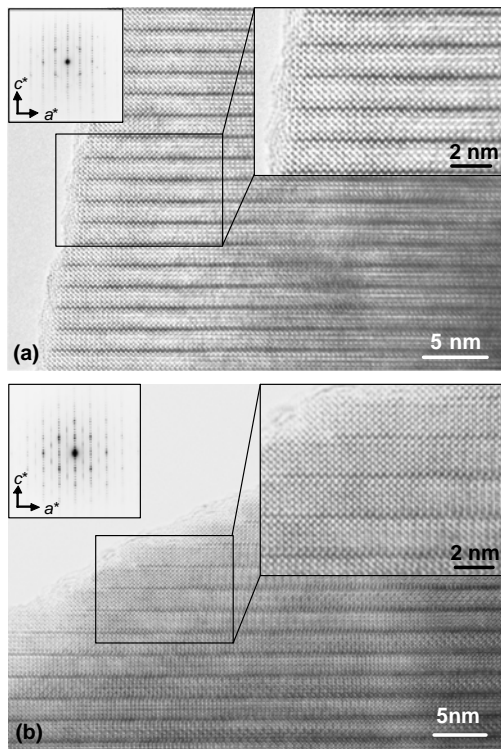


Fig. 4

